13 August 1999

ELSEVIER

Chemical Physics Letters 309 (1999) 198–208

CHEMICAL PHYSICS LETTERS

www.elsevier.nl/locate/cplett

Determination of the energy of the (d,d) electronic state involved in the radiationless deactivation of photoexcited nickel tetraphenylporphine

Pierre Brodard, Eric Vauthey *

Institute of Physical Chemistry of the University of Fribourg, Pérolles, CH-1700 Fribourg, Switzerland

Received 23 December 1998; in final form 28 April 1999

Abstract

The deactivation of the $S_1(\pi,\pi^*)$ excited state of nickel tetraphenylporphine has been investigated using various transient grating techniques. By measuring the density changes of the sample occurring during this process, the excited state, that is responsible for the ground state recovery time of 250 ps, was determined to lie 1.18 ± 0.13 eV above the ground state. This value suggests that this state is the ^{1}(d,d) state. © 1999 Elsevier Science B.V. All rights reserved.

1. Introduction

The crucial role played by porphyrins in many important biological processes has stimulated intensive chemical and photochemical investigations (see, e.g., Ref. [1]). The photophysical properties of metallo-porphyrins depend strongly on the nature of the metal in the core. When this metal is a closed-shell metal ion, the absorption and emission spectra of the porphyrins is almost fully determined by the π electrons of the porphyrin ring. These metallo-porphyrins, which are often termed regular porphyrins, exhibit fluorescence [1]. The presence of open-shell metal ions in the porphyrin core can lead to additional transitions which can be metal centred, metal to porphyrin or porphyrin to metal transitions. The presence of (d,d), (d,π^*) and (π,d) excited states resulting from these transitions below the (π,π^*) states of the porphyrin ring can offer an efficient pathway for the non-radiative deactivation from these porphyrin excited states [2]. This can result to a total suppression of the fluorescence. Ni(II)-porphyrins are such radiationless porphyrins, which have been very intensively investigated [3–7]. Ni(II)-porphyrins have d^8 configuration, with six electrons filling the d_{xy}, d_{xz} and d_{yz} orbitals. In the four-coordinated state, the two remaining electrons occupy the d_{z^2} orbital. The lowest excited state of this molecule is due to a transition of an electron from the d_{z^2} orbital to the empty $d_{x^2-y^2}$ orbital. The energy of this ^{1}(d,d) excited state and that of the corresponding triplet state ^{3}(d,d) are not known, as no band to due the (d,d) transition can be observed in the absorption spectrum [2]. Indeed, the first absorption

* Corresponding author. Fax: +41 26 3009737; e-mail: eric.vauthey@unifr.ch

0009-2614/99/$ - see front matter
PII: S0009-2614(99)00679-X

band of Ni(II)-porphyrins is the Q-band of the porphyrin ring, with a maximum between 520 and 550 nm. The resulting excited state is often labelled $S_1(\pi,\pi^*)$ state.

Ultrafast measurements have revealed that ground state recovery after excitation in the Q band of Ni(II)-tetraphenylporphine (NiTPP) takes place with a time constant of about 250 ps. A transient absorption band with this lifetime has been measured by several groups and has been ascribed to the ^{1}(d,d) state by Kobayashi et al. [3] while Chirvonyi et al. as well as Kim et al. have assigned it to the ^{3}(d,d) state [4,8].

In this Letter, we report on a determination of the energy of the 250 ps transient of NiTPP using the ps transient density phase grating method [9,10]. In a transient grating experiment [11,12], excitation is achieved by two laser pump pulses brought into interference in the sample. This results into a spatially modulated excitation intensity and thus to grating-like distributions of ground and excited state populations. Consequently, optical properties, like absorbance and refractive index are also spatially modulated. Any heat releasing process taking place from the excited state, like an internal conversion or an exothermic reaction, leads to a spatial distribution of temperature, which is accompanied by a spatial modulation of the density, hence of the refractive index. The amplitudes of these absorbance and refractive index modulations, called amplitude and phase gratings, respectively, can be probed by a third pulse, the probe pulse, striking the gratings at Bragg angle, θ_B. The intensity of the diffracted pulse, the signal, is related to the peak to null variation of the refractive index, Δn, and of the attenuation index, ΔK, as [13]:

$$\frac{I_{dif}}{I_{pr}} \cong \exp\left(-\frac{A \ln 10}{2\cos\theta_B}\right)\left(\frac{\pi l}{\lambda_{pr}\cos\theta_B}\right)\left[\Delta K_p^2 + \left(\Delta n_p + \Delta n_d\right)^2\right], \quad (1)$$

where I_{dif} and I_{pr} are the intensity of the signal and probe pulse, respectively, l is the sample thickness, Δn_p and Δn_d are the variations of the refractive index related to population and density changes, respectively, ΔK_p is the variation of the attenuation index due to the modulation of the populations, and A is the average absorbance of the sample at the probe wavelength, the relationship between the absorbance and the attenuation index being $K = A \ln 10 \lambda_{pr}/4\pi l$. The variation of the attenuation index due to density change, ΔK_d, can be neglected.

While other photo-thermal methods, like the thermal lens technique and the photoacoustic spectroscopy are limited to processes longer than about 100 and 10 ns, respectively [14], the density phase grating technique can resolve heat releasing processes taking place in less than 100 ps [15].

2. Experimental

2.1. Apparatus

The optical arrangement for the transient density phase grating measurements is depicted in Fig. 1. The second harmonic at 532 nm of a passive/active mode-locked and Q-switched Nd:YAG laser (Continuum PY61-10) was split into three parts with relative intensities of 10:10:1. The two most intense pulses were crossed in the sample using a nearly counter-propagating geometry. In this case, the fringe spacing, Λ, is given by:

$$\Lambda = \frac{\lambda_{pu}}{2\left[n^2 - \cos^2(\theta/2)\right]^{1/2}}, \quad (2)$$

where λ_{pu} is the pump wavelength, n is the refractive index of the sample and θ is the crossing angle of the pump pulses.

For probing, the weakest pulse was sent along a variable optical delay line before striking the grating at Bragg angle. The intensity of the diffracted pulse was measured with a vacuum photodiode. At each position of

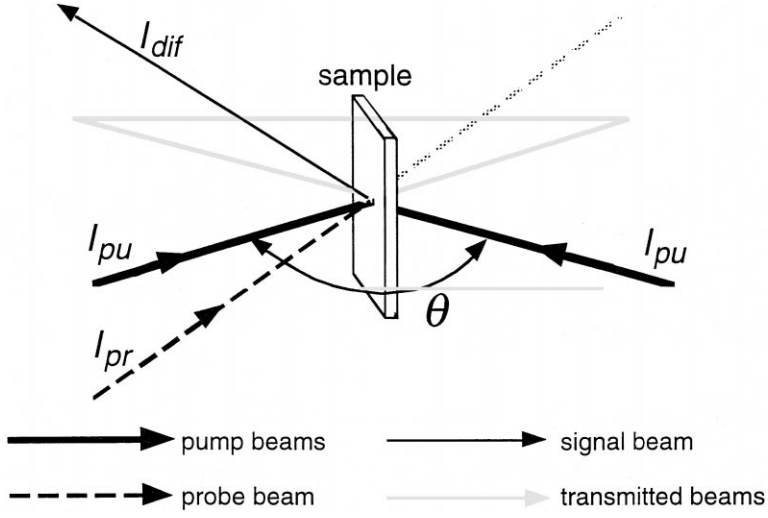

Fig. 1. Laser beam geometry for the density phase grating measurements.

the delay line, the diffracted intensity was averaged over 10 laser pulses. For each measurement, the delay line was scanned 20 times. Each measurement was repeated three times. The total pump intensity on the sample was about 500 $\mu J/cm^2$. At this regime, the shape of the signal time profile was independent of the intensity.

The temporal width of the laser pulse was 25 ps, as determined from the time profile of the diffracted intensity measured in neat CS_2 with focused beams. In this case, the polarisations of the pump pulses were perpendicular to each other, in order to avoid the formation of a phase grating through electrostriction [16].

The experimental setup for recording transient grating spectra has been described in details elsewhere [17,18]. Excitation was performed at 355 nm and a white light continuum generated by self phase modulation in a 60:40 (v/v) D_2O/H_2O mixture was used for probing.

2.2. Samples

Ni(II)-tetraphenylporphine (NiTPP) was prepared from the free-base tetraphenylporphine and was subsequently purified by column chromatography. Toluene (TOL), tetrahydrofuran (THF), dichloromethane (DCM) and 1,2-dichloroethane (DCE) were of spectroscopic grade and were used without further purification. The absorbance of the sample solution at the excitation wavelength was around 0.15 over 1 mm, the sample thickness. During the experiments, the sample solutions were continuously stirred by N_2 bubbling. No sample degradation was observed after the measurements. All experiments were performed at 20 ± 1°C.

3. Results and discussion

Fig. 2 shows the time profiles of the diffracted intensity at 532 nm measured with solutions of NiTPP in four different solvents. For these measurements, the crossing angle between the pump pulses was around 150° in air and about 160° in the sample. These time profiles look substantially different although the samples differ through the solvent only. The continuous line is the best fit of the following expression to the data [19,20]:

$$I_{\mathrm{dif}}(t) = C\int_{-\infty}^{+\infty} I_{\mathrm{pr}}(t-t')\,|\Delta\tilde{n}(t')|^2\,\mathrm{d}t', \tag{3}$$

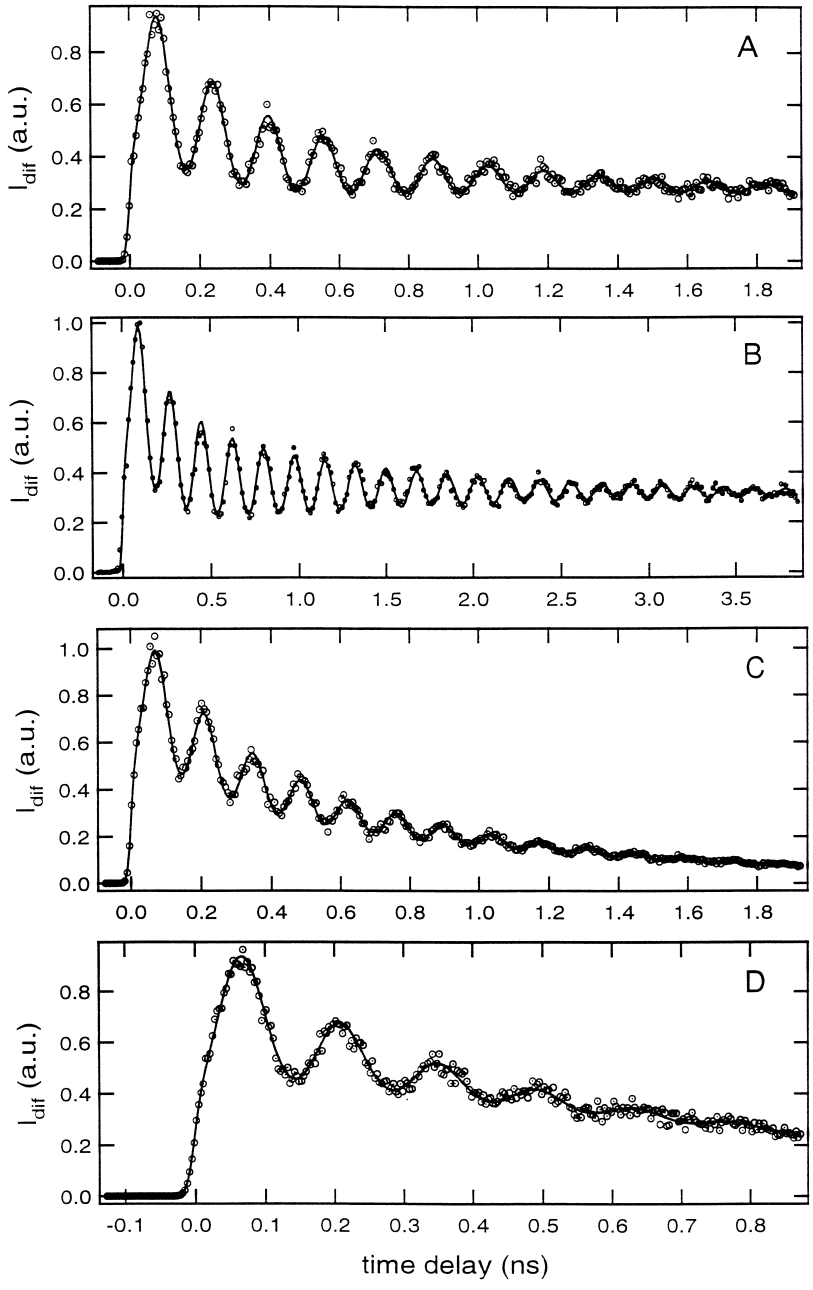

Fig. 2. Time profiles of the diffracted intensity measured at 532 nm upon excitation at 532 nm of solutions of NiTPP in (A) DCE, (B) DCM, (C) THF and (D) TOL. The continuous line is the best fit of Eq. (3).

where C is a constant, $I_{pr}(t)$ is the time profile of the probe intensity and $\Delta\tilde{n}$ is the modulation amplitude of the complex refractive index. The latter can be expressed as a sum of real and imaginary components:

$$\Delta\tilde{n}(t) = \Delta n_d(t) + \Delta n_p(t) + i\Delta K_p(t)\,. \tag{4}$$

In the data shown in Fig. 2, the diffracted intensity has two origins: (1) the population grating that contributes through both attenuation and refractive index changes, ΔK_p and Δn_p, respectively, and (2) the density grating that contributes through refractive index changes, Δn_d, the absorbance changes due to density variations, ΔK_d, being negligible.

3.1. Contribution of population gratings

The variation of the attenuation index in the 450–650 nm region has been measured by transient absorption spectroscopy and is shown in Fig. 3A. This transient spectrum is similar to that reported in the literature and consists of a dispersive like band which has been ascribed to the absorption of the (d,d) excited state [3–5,21]. Fig. 3C shows the transient grating spectrum due to population changes 60 ps after excitation at 355 nm. In order to avoid the contribution of the density grating, the crossing angle of the pump pulses was 0.3°. With this geometry the density grating is only formed after several ns. As explained in detail in Ref. [17], such a transient grating spectrum contains the square of the transient absorption spectrum, $\Delta K_p^2(\lambda_{pr})$, plus the square of the transient dispersion spectrum, $\Delta n_p^2(\lambda_{pr})$. Fig. 3A also shows the transient dispersion spectrum calculated by Kramers–Kronig transformation of the transient absorption spectrum. These two spectra were then used to calculate a transient grating spectrum (see Fig. 3B) which is in good agreement with the measured one (see Fig. 3C).

The time dependence of the population gratings has been measured using the same setup as for the data shown in Fig. 2 but using the crossed grating geometry, i.e., the polarisations of the pump pulses were perpendicular to each other as were the polarisation of the signal with respect to that of the probe pulse. In this case, the diffracted intensity, I_{dif}^{cros}, is proportional to the square of the linear dichroism and birefringence of the sample, which can decay by both population relaxation, with a rate constant k_{pop}, and rotational reorientation of the molecules with a rate constant k_{rot} [22]:

$$I_{dif}^{cros}(t) = I_{dif}^{cros}(0)\exp\left[-2\left(k_{pop} + k_{rot}\right)t\right]. \tag{5}$$

In order to eliminate the latter process from the decay of the diffracted intensity, the measurements were performed in castor oil, a highly viscous solvent ($\eta = 6$–8 P). The observed decay of I_{dif}^{cros} is indeed monoexponential resulting in a rate constant k_{pop} of $(4.0 \pm 0.2) \times 10^9$ s^{-1} (see Fig. 3D). The initial spike is partially due to optical Kerr effect of the solvent. The maximum polarisation anisotropy for a molecule like NiTPP with two perpendicular transition dipoles amount to 0.1. This implies that $I_{dif}^{cros}(0)$ is 16 times weaker than the initial diffracted intensity measured with parallel polarisation [22]. Therefore, these crossed grating measurement requires a higher pump intensity. A similar decay time was obtained in THF using the time dependence of the transient grating spectrum shown in Fig. 3B. Moreover, the same value has been measured in benzene and toluene [6]. Thus, the decay of the (d,d) state to the ground state can be considered to be independent of the solvent.

Consequently, the time dependence of ΔK_p and Δn_p can be expressed as:

$$\Delta n_p(t) = A_{np}\int_{-\infty}^{t} \exp\left(-k_{pop}(t-t')\right) I_{pu}(t')\,dt', \tag{6a}$$

$$\Delta K_p(t) = A_{Kp}\int_{-\infty}^{t} \exp\left(-k_{pop}(t-t')\right) I_{pu}(t')\,dt', \tag{6b}$$

where A_{np} and A_{Kp} are two amplitude factors and $I_{pu}(t)$ is the time profile of the pump intensity.

Fig. 3C shows that the contribution of the population grating to the diffracted intensity could be eliminated or at least strongly minimised by probing above 600 nm. However, considering the fringe spacing of the gratings formed with the setup shown in Fig. 1, Bragg diffraction is no longer possible for a probe wavelength longer than about 545 nm. Bragg diffraction at 600 nm would require a larger fringe spacing, that would lead to an unwanted decrease of the time resolution of the density phase grating experiment.

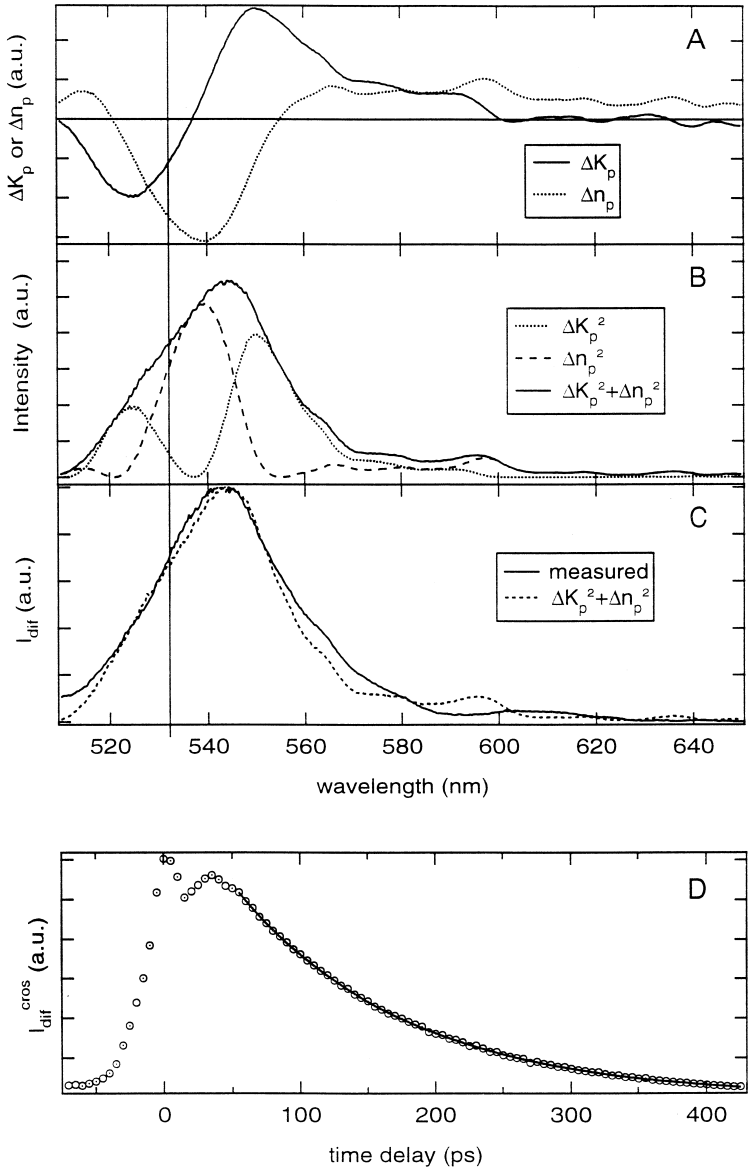

Fig. 3. (A) Transient absorption spectrum measured 60 ps after excitation at 355 nm and corresponding dispersion spectrum calculated by Kramers–Kronig transformation of the absorption spectrum. (B) Transient grating spectrum calculated from the measured absorption spectrum and the calculated dispersion spectrum. (C) Transient grating spectrum measured 60 ps after excitation at 355 nm together with the calculated one. (The vertical line corresponds to 532 nm, the pump and probe wavelength.) (D) Time profile of the diffracted intensity at 532 nm measured using the crossed grating geometry and best single exponential fit (continuous line).

3.2. Contribution of the density grating

The solvent dependence of the shape of the time profiles shown in Fig. 2 is thus due to the contribution of the density grating. The formation of this density grating occurs in two different time scales as shown in

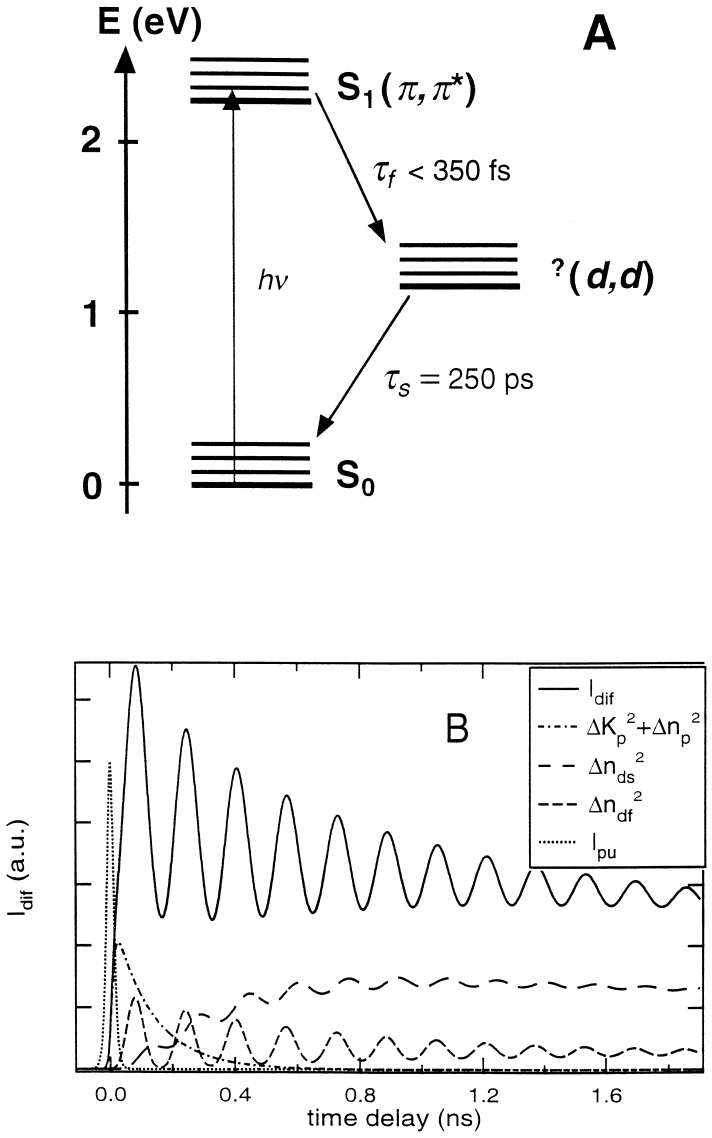

Fig. 4. (A) Electronic states involved in the ground state recovery of NiTPP after excitation at 532 nm. (B) Time profiles of the diffracted intensity due to the phase grating generated by the slow (Δn_{ds}) and fast (Δn_{df}) heat releases as well as to the population gratings ($\Delta n_p + \Delta K_p$), calculated using the parameters obtained from the analysis of NiTPP in DCE (see Fig. 2A).

Fig. 4A. In the fastest one, the heat release is due to the dissipation of the excess excitation energy and to the formation of the (d,d) state which has been reported to take place in less than 1 ps [6]. Non-radiative transition from the (d,d) state to the ground state results in a slower heat release with a rate constant of 4 ns^{-1}. Therefore, the time dependence of Δn_d is given by:

$$\Delta n_d(t) = \sum_{i=f,s} A_{di} \int_{-\infty}^{t} F_i(t-t') I_{pu}(t') \, dt, \tag{7}$$

where A_{df} and A_{ds} are amplitude factors [23]:

$$A_{df} \propto (X_s Q_f - \Delta V), \tag{8a}$$

$$A_{ds} \propto (X_s Q_s + \Delta V), \tag{8b}$$

with

$$X_s = \beta / \rho C_v,$$

and where Q_f and Q_s are the amount of heat released in the fast and slow processes, respectively, β is the coefficient of thermal expansion of the solvent with a density ρ and a heat capacity C_v. ΔV is the volume difference between NiTPP in the (d,d) state and in the ground state. This volume also comprises the solvation layer.

Finally, $F_i(t)$ is a shape function, which depends on the speed of sound in the sample, v_s, on the acoustic frequency, ω_{ac}, on the acoustic attenuation constant, α_{ac}, on the rate constant of thermal diffusion, k_{td}, and on the rate constant of the heat releasing process, k_i [15]:

$$F_i = \frac{k_{th}\omega_{ac}^{-1}\sin(\omega_{ac}t)\exp(-\alpha_{ac}v_s t) - \cos(\omega_{ac}t)\exp(-\alpha_{ac}v_s t) + \exp(-k_{td}t)}{k_{td}^2 + \omega_{ac}^2} - \frac{k_i\omega_{ac}^{-1}\sin(\omega_{ac}t)\exp(-\alpha_{ac}v_s t) - \cos(\omega_{ac}t)\exp(-\alpha_{ac}v_s t) + \exp(-k_i t)}{k_i^2 + \omega_{ac}^2}. \tag{9}$$

For example, the fast oscillation in the data of Fig. 2 is due to processes taking place faster than the acoustic period, $\tau_{ac} = 2\pi/\omega_{ac} = \Lambda/v_s$, which corresponds to the time needed for the density change to take place. In this case, the time profile of the diffracted intensity is driven by the acoustic response of the system and exhibits oscillation at the acoustic period. The damping of the oscillation is due to acoustic attenuation which, as shown in Fig. 2, varies from one solvent to the other.

For the fit of Eq. (3), six parameters were adjusted: the acoustic frequency, ω_{ac}, the acoustic attenuation constant, α_{ac}, the rate constant of thermal diffusion, k_{td}, the amplitude factors related to the fast and slow density changes, A_{df} and A_{ds}, and the amplitude factor, A_{pK}, due to the contribution of ΔK_p. The other parameters were fixed: the amplitude factor related to Δn_p was taken as $A_{pn} = 2.14A_{pK}$, as determined from the spectra shown in Fig. 3, k_f was taken as 1 ps^{-1} and the measured value of $k_{pop} = 4$ ns^{-1} was used for k_s. The pump and probe pulse profiles, $I_{pu}(t)$ and $I_{pr}(t)$, were described as a $sech^2$ function with a width of 25 ps (FWHM), as measured by optical Kerr effect in CS_2.

The values of some of the adjustable parameters obtained from the fit are listed in Table 1 together with X_s and the speed of sound. This table shows that the solvent dependence of the time profiles shown in Fig. 2 is not due to the relative magnitude of the fast and slow heat releasing processes, but only to the thermoacoustic

Table 1
Amplitude ratio f, acoustic attenuation constant, α_{ac}, and acoustic period, τ_{ac} obtained from the fit of Eq. (3) to the measured time profiles of the diffracted intensity in various solvents, together with the thermal expansivity, X_s and speed of sound, v_s

Solvent	X_s [a] (ml kJ^{-1})	f	$\alpha_{ac}v_s$ (ns^{-1})	τ_{ac} (ps)	v_s (m s^{-1})
DCE	0.706	0.52 ± 0.05	1.5	158	1216 [24]
DCM	0.875	0.51 ± 0.05	0.7	176	1093 [24]
THF	0.657	0.51 ± 0.05	2.4	138	1311 [25]
TOL	0.742	0.50 ± 0.05	3.0	142	1327 [26]

[a] Values of β were taken from Ref. [27] (DCE, DCM), Ref. [28] (THF) and Ref. [29] (TOL). Values for ρ and C_v where taken from Ref. [30].

properties of the solvents. The rate constant of thermal diffusion, which is responsible for the decay of the thermal component of the density grating, could not be determined accurately from the time profile because of the relatively small time window of the experiment. The k_{td} values obtained from the fit lies between 0.01 and 0.1 ns^{-1}. The magnitude of this parameter as well as that of α_{ac} depends on the fringe spacing. Nevertheless, these values are in reasonable agreement with those measured using different experimental geometries [31,32]. Moreover, the acoustic frequencies and the acoustic attenuations constants in DCE and DCM are very similar (within 10%) to those measured independently with malachite green. In non viscous solvents, this dye is known to have an excited lifetime of a few ps, due to a very efficient internal conversion to the ground state. However, these measurements could not be performed in TOL and THF, because of the low solubility of malachite green.

Fig. 4B shows the calculated time profiles of the diffracted intensity due to the phase grating generated by the fast and slow heat releases as well as the total contribution of the population gratings ($\Delta n_p + \Delta K_p$) using the parameters obtained from the fit of NiTPP in DCE (see Fig. 2A). It can be seen that the time profiles due to the fast and slow heat releases are very different. This is due to the large crossing angle of the pump pulses, which results in acoustic periods that are substantially shorter than the decay time of the (d,d) state. The signal originating from the fast heat release reaches its maximum in half an acoustic period, in about 70 ps in the present case. On the other hand, the signal due to population grating reaches its maximum earlier (around 20 ps). This difference in the rise time, which can be observed in initial part of the time profiles shown in Figs. 2 and 4B, allows an estimation of the contribution of the population grating to the signal. From the fit, the magnitude of this relative contribution is the largest in THF and the smallest in DCM, as expected from the X_s values of the solvents (see Table 1).

As shown in Eqs. (8a) and (8b), the modulation of density can also be caused by structural volume changes, ΔV. The latter can be determined from the variation of the relative magnitude of $A_{d,f}$ and $A_{d,s}$ with the solvent parameter X_s as proposed by Zimmt and co-workers [31]:

$$fX_sQ_{tot} = X_sQ_s + \Delta V\,, \tag{10}$$

where $f = A_{ds}/(A_{df} + A_{ds})$ and $Q_{tot} = Q_f + Q_s$. As all the optical excitation energy is converted into heat, Q_{tot} amounts to 337 kJ mol^{-1}. From Eq. (10), a plot of fX_sQ_{tot} vs. X_s should result in a straight line with a slope equal to Q_s and an intercept corresponding to ΔV. Fig. 5 shows such a plot with the best linear fit.

Because of the relatively large X_s values of the solvents, the error on the volume change is large. Findsen et al. have reported that the resonance Raman spectrum of Ni-porphyrins in the (d,d) state is very similar to the ground state one, except that all the bands exhibit a shift to lower frequency [33]. From these shifts, an average

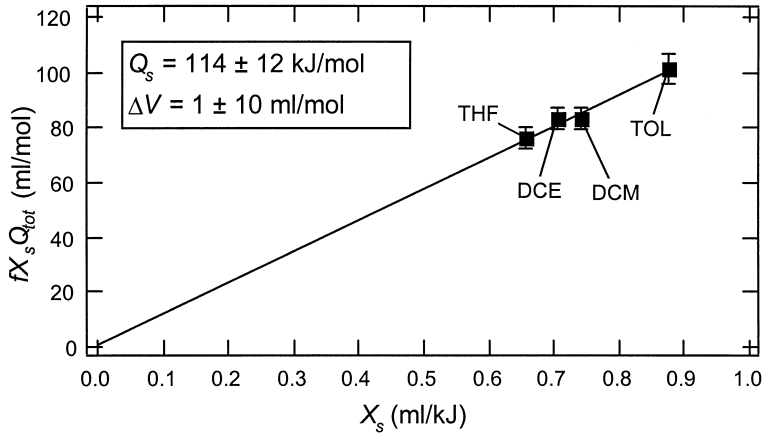

Fig. 5. Molar expansion accompanying the radiationless decay of the (d,d) state of NiTPP as a function of the solvent parameter X_s.

increase of the C–C bond length by about 2% was determined. This ring expansion was explained by the promotion of an electron to the $d_{x^2-y^2}$ orbital, hence to an increase of the in-plane electron density. Using this value and assuming that the porphyrin is a disk with a thickness of 3.5 Å results in a structural volume change ΔV of about 7 ml mol^{-1}, i.e., within the error limit on the intercept. The contribution of solvent to the volume change can be expected to be of minor importance. Indeed, as the excitation is localised on the metal, there is no change in the electronic distribution that could lead to a noticeable variation of the volume via electrostrictive effects.

The slope obtained from the plot in Fig. 5 indicates that the (d,d) state, which decays in 250 ps, lies 1.18 ± 0.13 eV (114 ± 12 kJ/mol) above the ground state. The spin multiplicity of this state is still unclear: according to Kobayashi et al. the 250 ps transient is a singlet state [3], while Chirvonyi et al. [8] as well as Kim et al. [4] have assigned it to a triplet state. The latter authors arrived at this conclusion by assigning changes observed in the red part of the transient spectrum taking place in the first few ps after excitation to the formation of the ^{3}(d,d) state by intersystem crossing from the ^{1}(d,d) state [4]. However, this investigation was performed with 30 ps pulses. More recently, Rodriguez and Holten have studied the excited dynamics of NiTPP using 350 fs pulses [6]. These authors concluded that the 250 ps (d,d) state is generated in less than 350 fs and that the spectral changes initially assigned to the formation of the ^{3}(d,d) state were rather due to vibrational cooling to the thermalised (d,d) state [6]. Moreover, their measurements did not allow to draw any conclusion on the spin multiplicity of this state.

According to extended Hückel calculations, the energy gap between the singlet and triplet (d,d) states of four-coordinated, square planar Ni complexes amounts to 0.8 eV [34]. If the 250 ps transient is the ^{1}(d,d) state, the ^{3}(d,d) state would lie 0.38 eV above the ground state, which is, according to Ake and Gouterman [34], physically reasonable. In this case, the absorption band due to the (d,d) transition should be located between 950 and 1150 nm and could account for the long wavelength tail measured in the near IR region [2]. Higher level calculations, such as those based on density functional theory might allow a better assignment of the multiplicity of this transient. Time resolved ESR would be the only method to obtain an univocal experimental proof.

Acknowledgements

We wish to thank Dr. O. Mongin from the Institute of Organic Chemistry of the University of Fribourg for supplying the porphyrin. This work was supported by the Fonds National Suisse de la Recherche Scientifique through project number 20-49235.96 and by the ''programme d'encouragement à la relève universitaire de la Confédération''. Financial support form the Fonds de la Recherche and the Conseil de l'Université de Fribourg is also acknowledged.

References

[1] K. Kalyanasundaram, Photochemistry of Polypyridine and Porphyrin Complexes, Academic Press, San Diego, CA, 1992 (and references therein).
[2] A. Antipas, M. Gouterman, J. Am. Chem. Soc. 105 (1983) 4896.
[3] T. Kobayashi, K.D. Straub, P.M. Rentzepis, Photochem. Photobiol. 29 (1979) 925.
[4] D. Kim, C. Kirmaier, D. Holten, Chem. Phys. 75 (1983) 305.
[5] V.S. Chirvonyi, B.M. Dzhagarov, Y.V. Timinskii, G.P. Gurinovitch, Chem. Phys. Lett. 70 (1979) 79.
[6] J. Rodriguez, D. Holten, J. Chem. Phys. 91 (1989) 3525.
[7] H.S. Eom, S.C. Jeoung, D. Kim, J.H. Ha, Y.R. Kim, J. Phys. Chem. A 101 (1997) 3661.
[8] V.S. Chirvonyi, B.M. Dzhagarov, A.M. Shul'ga, G.P. Gurinovotch, Dokl. Akad. Nauk SSSR 259 (1981) 144.
[9] R.D.J. Miller, in: R.J.H. Clark, R.E. Hester (Eds.), Advances in Spectroscopy, vol. 18, Wiley, New York, 1989, p. 1.
[10] M. Terazima, Adv. Photochem. 24 (1998) 255.
[11] H.J. Eichler, P. Günter, D.W. Pohl, Laser-Induced Dynamic Gratings, Springer, Berlin, 1986.

[12] M.D. Fayer, Annu. Rev. Phys. Chem. 33 (1982) 63.
[13] H. Kogelnik, Bell. Syst. Tech. J. 48 (1969) 2909.
[14] S.E. Braslavsky, G.E. Heibel, Chem. Rev. 92 (1992) 1381.
[15] L. Genberg, Q. Bao, S. Gracewski, R.J.D. Miller, Chem. Phys. 131 (1989) 81.
[16] R.J.D. Miller, R. Casalegno, K.A. Nelson, M.D. Fayer, Chem. Phys. 72 (1982) 371.
[17] C. Högemann, M. Pauchard, E. Vauthey, Rev. Sci. Instrum. 67 (1996) 3449.
[18] E. Vauthey, C. Högemann, X. Allonas, J. Phys. Chem. A 102 (1998) 7368.
[19] J. Etchepare, G. Grillon, J.P. Chambaret, G. Hamoniaux, A. Orzag, Opt. Commun. 63 (1987) 329.
[20] F.W. Deeg, M.D. Fayer, J. Chem. Phys. 91 (1989) 2269.
[21] J. Rodriguez, C. Kirmaier, D. Holten, J. Am. Chem. Soc. 111 (1989) 6500.
[22] A.B. Myers, R.M. Hochstrasser, IEEE J. Quantum Electron. QE-22 (1986) 1482.
[23] J. Morais, M.B. Zimmt, J. Phys. Chem. 99 (1995) 8863.
[24] R.T. Lagemann, J.S. Evans, D.R. McMillan Jr., J. Am. Chem. Soc. 70 (1948) 2997.
[25] N.B. Lezhnev, Z.B. Fainberg, N.P. Erchak, E. Lukevics, Russ. J. Phys. Chem. 56 (1982) 388.
[26] F.C. Collins, M.H. Navidi, J. Chem. Phys. 22 (1954) 1254.
[27] J. Nath, J. Chem. Thermodyn. 28 (1996) 481.
[28] G. Korösi, E. Sz. Kovatz, J. Chem. Eng. Data 26 (1981) 323.
[29] S.C. Sharma, M.L. Lakhanpal, M.L. Rumpaul, Ind. J. Chem. 21 (1982) 67.
[30] J.A. Riddick, W.B. Bunger, Organic Solvents, Wiley, New York, 1970.
[31] J. Morais, J. Ma, M. Zimmt, J. Phys. Chem. 95 (1991) 3885.
[32] E. Vauthey, A. Henseler, J. Phys. Chem. 100 (1996) 170.
[33] E.W. Findsen, J.A. Shelnutt, M.R. Ondrias, J. Phys. Chem. 92 (1988) 307.
[34] R.K. Ake, M. Gouterman, Theor. Chim. Acta 17 (1970) 408.